Feature value detection from high-speed observation of spatter for prediction of porosity in metals formed using powder bed fusion

Ryo Okawara[1,#], Moju Zhao[1], Justin Lach[1], Hiroshi Yoshizaki[2], Masahiko Sairaiji[2], Masayuki Nakao[1] and Keisuke Nagato[1]

1 Department of Mechanical Engineering, The University of Tokyo, 7-3-1 Hongo, Bunkyo-ku, Tokyo, 113-8656, Japan
2 SOLIZE Corporation, Sanban-cho UF Bldg. 3F, 6-3, Sanban-cho, Chiyoda-ku, Tokyo, 102-0075, Japan
Corresponding Author / Email: okawara@hnl.t.u-tokyo.ac.jp, TEL: +81-3-5841-6362

KEYWORDS: Powder bed fusion, Porous, Spatter, High-speed observation

Porous metals are widely used in industry for lightweight parts and heat exchangers. Controlling porosity and pore size is crucial for enhancing the performance of these materials. Powder bed fusion (PBF) offers a promising approach for achieving such control, but the search for optimal parameters is time-consuming and challenging due to the vast parameter space. Simulating the thermofluidic dynamics of the complex phenomena occurring at the laser spot is equally difficult. In this study, we used Bayesian optimization to explore process parameters for porous materials. Bayesian optimization optimizes the objective function with minimal trials of parameters. However, obtaining the porosity and pore size as objective functions requires time due to the fabrication of bulk samples and cross-sectional observations. Therefore, we propose and develop a method using intermediate features to predict capillary efficiency, reducing the trial cycle time. Optimizing the area in which the number of spatter counts are taken improves the accuracy of predicting the peak capillary efficiency.

1. Introduction

Porous materials are widely used in industry. To improve the performance of these porous materials, it is important to control the porosity and pore size to the desired level. However, the Powder Bed Fusion (PBF) method [1,2], which is a production method for porous bodies, has many process parameters and is a very complex phenomenon, requiring a great deal of time and effort to find parameters to obtain the desired mechanical properties.

To address this problem, research has been conducted to apply Bayesian optimization to the process parameter search [3,4]. However, conventional Bayesian optimization has a problem in that the cycle time required for parameter search is long because the PBF method requires time for stacking and measuring the characteristic values [5].

In this study, we propose extracting intermediate features to be added to the Bayesian optimization and to develop a method to reduce the cycle time for parameter determination as shown in Fig. 1. This will speed up process parameter determination for high-performance metal porous body fabrication.

2. Method

2.1 Methods and conditions for high-speed observation

Fig. 2 shows the experimental system, in which a sample of SUS316 powder was laid on SUS316 bulk, the powder was irradiated by a CW laser (MF-C500A-SF, AMADA WELD TECH Co., Ltd.) and photographed using a high-speed camera (FASTCAM Nova S16, Photron Ltd.) and laser illumination (CAVILUX HF, Cavitar Ltd.) The particle size distribution of the powder (Sanyo Special Steel Co., Ltd., PSS316L) used was D10=6.241 μm, D50=11.46 μm, D90=20.53 μm. Note that D10, D50, and D90 indicate diameters corresponding to 10%, 50%, and 90% of the integrated distribution. The laser power was 100 W, 150 W, 200 W, 250 W, 300 W, scanning speeds of 600 mm/s, 900 mm/s, 1200 mm/s, 1500 mm/s, 1800 mm/s, with a spot diameter of 150 μm, and powder layer thickness of 50 μm.

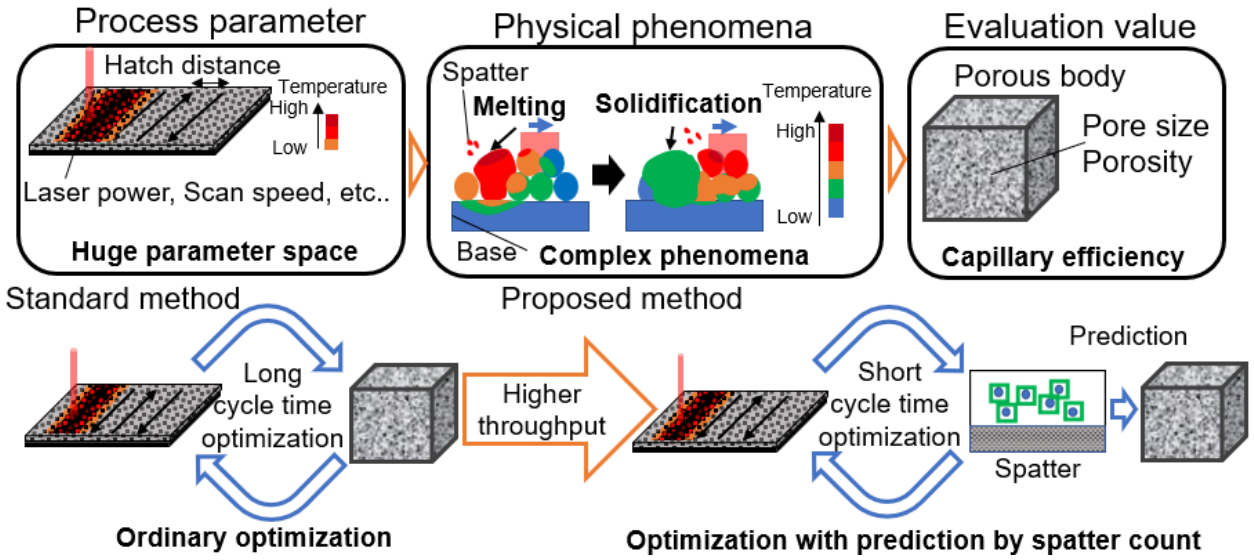

Fig. 1 Schematic of usage of feature value from high-speed observation of spatter

In order to obtain the spatter distribution, which is caused by the direction and velocity of the spatter, we divided the video into three regions and measured the number of spatter particles using image processing. The laser scanned rightward within the shooting range, and the spatter was mainly scattered to the left side of the laser. Fig. 3 shows a schematic diagram of the region division, and Table 1 shows the conditions for the angle of the dividing line.

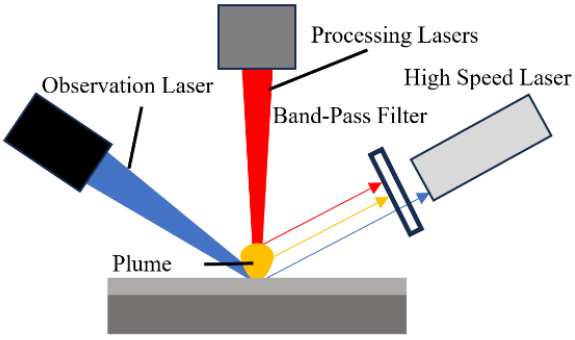

Fig. 2 Schematic diagram of the experimental system

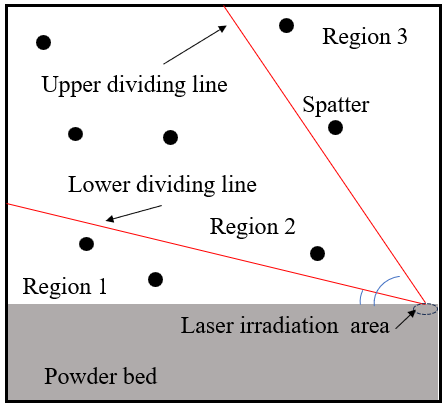

Fig. 3 Schematic diagram of the region division

Table 1 conditions for the angle of the dividing line

Lower dividing line[°] \ Upper dividing line[°]	10	20	30	40	50	60
10	-	○	○	○	○	○
20	-	-	○	○	○	○
30	-	-	-	○	○	○
40	-	-	-	-	○	○
50	-	-	-	-	-	○
60	-	-	-	-	-	-

2.2 Method and conditions for capillary efficiency calculation

Porous samples were fabricated using a metal 3D printer (ProX 300,3D Systems Corporation), mechanical properties were measured, and capillary efficiency was calculated. The modeling conditions were the same as in the experiment, and 25 samples were created. Porosity and pore size were measured for mechanical properties. Porosity was calculated by dividing the weight of the porous part of the sample by the weight of the same volume in bulk, and pore sizes were measured by the bubble point method. The capillary efficiency coefficient E was calculated as follows. The physical quantities and units for each symbol are as shown in Table 2. The capillary efficiency coefficient E can be expressed using the capillary pressure ΔP and permeability K as in Equation 1 [6].

$$E = \Delta P \cdot K \tag{1}$$

The capillary pressure ΔP can be expressed by the Young-Laplace equation using the surface tension σ, contact angle θ, and pore size r as in Equation 2, and the permeability K can be expressed by the Kozeny-Kalman equation using the constant C_1, shape constant τ, porosity ε, and grain size d as in Equation 3.

$$\Delta P = \frac{2\sigma \cos\theta}{r} \tag{2}$$

$$K = \frac{C_1 \cdot \varepsilon^3 \cdot d^2}{\tau \cdot (1-\varepsilon)^2} \tag{3}$$

The porosity ε is simply expressed as in Equation 4 using the pore

size r and grain size d. From Equations 1, 2, 3, and 4, the capillary efficiency coefficient E can be expressed as in Equation 5 using the pore size r, porosity ε, and constant C_2. In this study, the constant C_2 in Equation 5 was set to 1×10^6 for simplicity and the capillary efficiency coefficient was calculated.

$$\varepsilon = \frac{r^2}{r^2 + d^2} \tag{4}$$

$$E = \frac{C_2 \cdot r \cdot \varepsilon^2 \cdot (1+\varepsilon)}{(1-\varepsilon)^2} \tag{5}$$

Table 2 Physical quantity and unit for each symbol

Symbol	Physical quantity	Unit
E	capillary efficiency coefficient	N
ΔP	capillary pressure	Pa
K	permeability	m^2
σ	surface tension	N/m
θ	contact angle	rad
ε	porosity	-
d	grain size	m
τ	shape constant	-
r	pore size	m
C	constant	-

3. Results

Spatter was detected from the captured images by image processing. Fig. 4 shows the results of the spatter detection image processing. Each particle of spatter is surrounded by a rectangle and unmelted particles on the sample are not mistakenly detected as spatter.

The number of spatter particles scattering in regions 1 and 3 were added together and compared to the capillary efficiency coefficient as a feature value. If the peak positions are close to each other, the feature is found to be suitable as an intermediate feature.

The coefficient of determination R^2 and an original evaluation value were calculated as a measure to evaluate the features.

Fig. 5 shows the contour plots of the Gaussian regression process after calculating the coefficient of determination for 15 conditions in which the angle of the dividing line was varied. The results of the Gaussian regression process show that an angle of the top and bottom dividing lines of 65° and 32°, respectively, are the most similar to the capillary efficiency coefficient and are optimal. The coefficient of determination in this case is higher than the coefficient of determination when the number of spatter particles in all regions are used as a feature without the dividing line, thus the dividing line works to improve the accuracy. However, the coefficient of determination was affected by values other than the peak, resulting in a much smaller coefficient of determination.The original evaluation value was calculated as the percentage of areas where the normalized spatter count was greater than 0 among the areas where the capillary efficiency was greater than -0.3. The score for the method with no dividing line was 0.537, while the score for the method with the upper dividing line angle of 65° and the lower dividing line angle of 32° was 0.580, indicating that the accuracy had been improved.

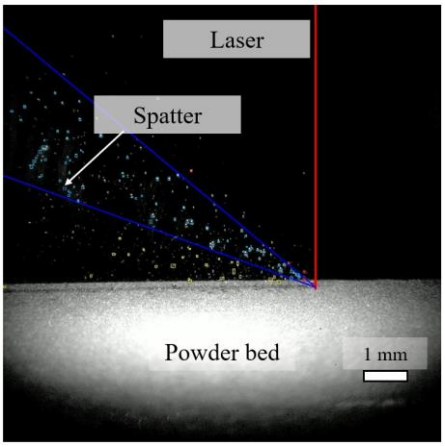

Fig. 4 Results of spatter detection image processing

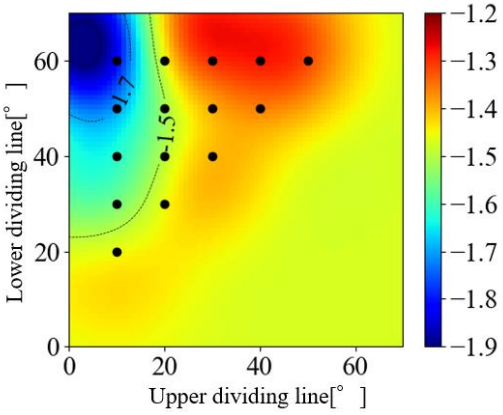

Fig. 5 Contour plot of R^2 with varying dividing line

4. Discussion

The reasons for the improvement in accuracy by adding Regions 1 and 3 together and excluding Region 2 are discussed. First, capillary efficiency increases under conditions of large porosity and small pore size. However, due to the mechanism of modeling, there is a trade-off between porosity and pore size. When the energy density is high, the porosity becomes too small, and when the energy density is low, the pore size becomes too large. In other words, capillary efficiency peaks when the energy density is moderate.

The spatter generation mechanism can be divided into the following branches depending on the energy density. Under low energy density conditions, spatter is thought to be generated by the mechanism shown in Fig. 6. The surface of the powder is melted by laser irradiation. The molten powder clumps together, but some of it is scattered by the updraft generated at the same time. As a result, large spatter is generated from multiple molten powder mixtures, which are dispersed in one direction of the updraft, with a narrow dispersal angle, and are considered to be dispersed mainly in region 2. In other words, the amount of spatter in regions 1 and 3, which are characteristic quantities, will be small. Under the condition of high energy density, spatter is

considered to be generated by the mechanism shown in Fig. 7. A melt pool is formed by laser irradiation, and recoil pressure is generated by metal evaporation [7]. The recoil pressure destabilizes the surface, and as a result, the molten metal from the melt pool is torn into small pieces, resulting in small spatter. As a result, small spatter is generated, and large spatter, as in the previous mechanism, is not primarily generated. The scattering angle depends on the surface from which the spatter originates and becomes wide. Although the scattering direction is wide, the amount of spatter is small to begin with because the inside of the melt pool is more stable than when the energy density is low. In other words, the amount of spatter scattered in regions 1 and 3, which are characteristic quantities, becomes small. Based on these mechanisms, the amount of spatter scattered in regions 1 and 3, is considered to peak at a medium energy density. For these reasons, it is considered that setting a dividing line for the amount of spatter would have improved the accuracy.

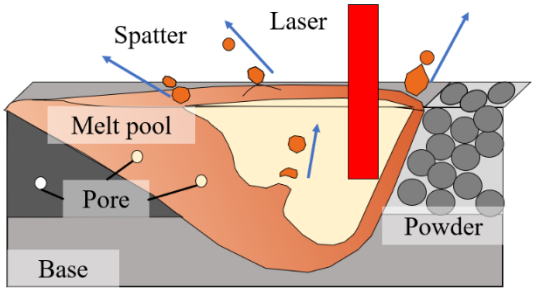

Fig. 6 Schematic diagram of spatter generation mechanism at low energy density

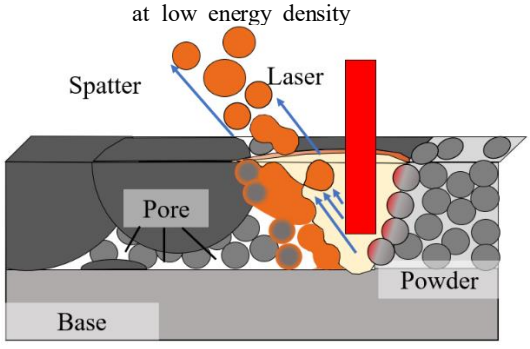

Fig. 7 Schematic diagram of spatter generation mechanism at high energy density

5. Conclusions

In this study, we developed a process to extract features that predict the capillary efficiency coefficient of a porous body in PBF, and considered the spatter particle count as a candidate. A dividing line was set, and optimization was performed for the angle of the dividing line. As a result, the accuracy was improved by setting the dividing line. In the future, it will be necessary to develop image processing technology to classify molten spatter and powder spatter, and to consider spatter size, spatter dispersion angle, and the dispersion of spatter location as feature quantities.

REFERENCES

1. Herzog D *et al.*, “Additive manufacturing of metals”, Acta Materialia 117(2016) 371–92.
2. MR. Alkahari *et al.*, “Consolidation characteristics of ferrous-based metal powder in additive manufacturing”, Journal of Advanced Mechanical Design, Systems, and Manufacturing 8 (2014) 1.
3. K. Nagai *et al.*, “Sample-efficient parameter exploration of the powder film drying process using experiment-based Bayesian optimization”, Scientific Reports 12 (2022) 1615.
4. G. Tapia *et al.*, “Gaussian process-based surrogate modeling framework for process planning in laser powder-bed fusion a dditive manufacturing of 316L stainless steel”, The Internatio nal Journal of Advanced Manufacturing Technology 94 (201 8) 3591-3603.
5. K. Nagato *et al.*, “Enhancing the prediction quality of mechanical properties for powder bed fusion with laser beam by dynamic observation of flying particles”, Material and Design 227 (2023) 111696.
6. D. Deng *et al.*, “Evaluation of capillary performance of sintered porous wicks for loop heat pipe”, Experimental Thermal and Fluid Science 50 (2013) 1-9.
7. H. Nakamura *et al.*, “Elucidation of melt flows and spatter formation mechanisms during high power laser welding of pure titanium”, Journal of Laser Applications 27 (2015) 3.